Analytica Chimica Acta 1093 (2020) 52–60

Contents lists available at ScienceDirect

Analytica Chimica Acta

journal homepage: www.elsevier.com/locate/aca

Ultrasensitive detection of miRNA based on efficient immobilization of probe and electrochemiluminescent quenching of $Ru(bpy)_3^{2+}$ by methylene blue

Liping Lu [a, *], Chang Liu [a], Wujian Miao [b, **], Xiayan Wang [a], Guanghsheng Guo [a]

[a] College of Environmental and Energy Engineering, Beijing University of Technology, Beijing, 100124, China
[b] Department of Chemistry and Biochemistry, The University of Southern Mississippi, Hattiesburg, MS, 39406, USA

HIGHLIGHTS

- The mechanism of the ECL quenching of $Ru(bpy)_3^{2+}$ by methylene blue was discussed.
- $Ru(bpy)_3^{2+}$ labeled DNA hairpin probe was assembled through click chemistry.
- A binding constant of miRNA with DNA was estimated based Langmuir isotherm model.
- This miRNA biosensor manifests high sensitivity, specificity and reproducibility.
- Efficient determination of miRNA extracted from the A549 cell lines was conducted.

GRAPHICAL ABSTRACT

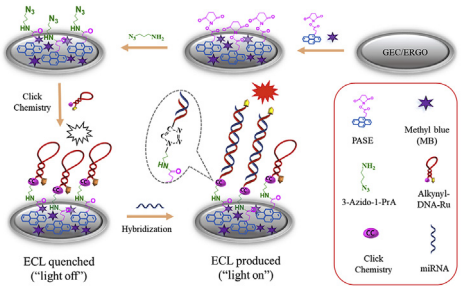

ARTICLE INFO

Article history:
Received 25 September 2019
Accepted 27 September 2019
Available online 5 October 2019

Keywords:
MicroRNA
ECL quenching
$Ru(bpy)_3^{2+}$
Methylene blue
Click chemistry

ABSTRACT

A high performance miRNA biosensor based on effective click chemistry assembly of a $Ru(bpy)_3^{2+}$ labeled DNA probe and efficient electrochemiluminescence (ECL) quenching of the $Ru(bpy)_3^{2+}$/BDEA (BDEA = N-butyldiethanolamine) system by surface-confined electroactive methylene blue (MB) dye is reported. When the target miRNA was present, the ECL signal instantly changed from "light off" to "light on" status. Using the specific miRNA let-7d as the target analyte, this biosensor provided sensitive detection over approximately six orders of magnitude (10 fM-10 nM), with a limit of detection of 10 fM (S/N = 3). Detailed study of the ECL quenching behavior of the $Ru(bpy)_3^{2+}$/BDEA system by MB in solution suggested that the ECL quenching involves a combination of photoluminescence dynamic quenching and quenching processes directly associated with the redox reactions, as well as resonance energy transfer. A large binding constant of $4.7 \times 10^{11}\ M^{-1}$ between let-7d and the DNA hairpin was estimated using an ECL-based extended Langmuir isotherm model, suggesting remarkably strong binding of the target to the probe. Furthermore, our biosensor exhibited excellent specificity and reproducibility. Using the developed system, the concentration of the target miRNA extracted from the A549 cell line could be obtained, demonstrating the potential application of the developed biosensor to practical biological sample analysis.

* Corresponding author.
** Corresponding author.
E-mail addresses: lipinglu@bjut.edu.cn (L. Lu), Wujian.Miao@usm.edu (W. Miao).

https://doi.org/10.1016/j.aca.2019.09.073
0003-2670/

1. Introduction

Mature microRNAs (miRNAs) are a class of evolutionally conserved, single-stranded, and small (19–23 nucleotides) non-protein-coding RNAs [1,2] that play a crucial role in gene expression for most eukaryotic organisms [3,4]. Recent studies have demonstrated that the abnormal expression of miRNAs is relevant to the origin and development of human diseases, genetic disorders, and altered immune system function [5–7]. Therefore, sensitive detection and quantification of miRNAs could provide major advantages for the early clinical diagnosis and treatment of certain types of diseases, especially cancers. A number of biosensor-based methods for the detection of miRNA use signal detection approaches including photoluminescence [8], field-effect transistors [9], or electrochemistry [10]. This is because miRNA biosensors are often considered to be easily constructed, cost-effective, portable, and highly sensitive [11–13]. To develop sensitive and accurate biosensors, the target recognition element (e.g., a DNA probe) should be attached to the substrate in such a way that the target (e.g., a complementary miRNA) can effectively hybridize with the probe and remain on the substrate over a number of detection cycles. For example, mercapto-DNA sequences have been frequently self-assembled on the surface of gold electrodes via Au–S bonds [14–16] for analysis of DNA or RNA targets; however, this type of assembly is often negatively affected by the uncontrollability of the monolayer composition, including the amount of DNA on the monolayer and its dispersibility [17,18], as well as by damage to the Au–S binding upon electrochemical oxidation, which could lead to detachment of the biosensing layer from the electrode [19]. Another key factor that profoundly affects the limit of detection is the sensing or detection technique used. Among the commonly used detection approaches, electrogenerated chemiluminescence (ECL) has proven to be one of the most sensitive and reproducible detection techniques compared to techniques such as enzyme-linked immunosorbent assay (ELISA), photoluminescence, chemiluminescence, and electrochemistry due to its unique mechanistic principles and inherent properties, which include specific light generation pathways, lack of background signals, and the possibility of manipulating the reaction [20–23]. Consequently, ECL-based biosensors have attracted great attention in the field of miRNA sensing [24–29]. Two general modes have been employed to correlate the concentration of the target with the resulting change in the ECL signal. The first mode can be regarded as the "ECL enhancement mode", in which the ECL signal increases proportionally with the analyte concentration, while the second mode or "ECL quenching mode" often involves a decrease in the ECL intensity of a known ECL system (e.g., $Ru(bpy)_3^{2+}$/TPrA) after the addition of an ECL quencher (e.g., ferrocene) [30–33]. When the analyte itself acts as the quencher, the ECL intensity of the test system decreases with increasing concentration of the analyte [34]. To obtain high sensitivity, several measures can be taken. For example, the ECL intensity can be enhanced by (a) using an ECL probe that contains both an ECL emitter and co-reactant groups in the same molecule to shorten the electronic transmission distance and improve the luminous stability [35], (b) adding an additional chemical to the detection system to promote ECL generation [36], or (c) in situ catalysis of the ECL with a high concentration of a self-generated co-reactant [29]. However, for the ECL quenching mode, the use of a highly efficient ECL quencher is an essential prerequisite to obtain an ultrasensitive biosensor.

Herein, we report the fabrication and application of an ECL quenching-based biosensor for the sensitive detection and quantification of miRNA let-7d extracted from human lung adenocarcinoma cell (A549) lysate. Two novel strategies, namely, (a) the use of click chemistry for the effective attachment of the DNA probe to the electrode and (b) the use of the electro-reactive dye methylene blue (MB) [37,38] as a highly efficient ECL quencher for the $Ru(bpy)_3^{2+}$/BDEA (BDEA = N-butyldiethanolamine) system, are employed. Scheme 1 depicts the preparation of the biosensor and its detection principle. Briefly, a layer of graphene oxide is electrochemically reduced and deposited on a glassy carbon electrode (GCE/ERGO), and a mixture of 1-pyrenebutyric acid N-hydroxysuccinimide (PASE) and MB is cast onto the layer. This is followed by the covalent attachment of 3-azido-1-propylamine (3-Azido-1-PrA) to the PASE linker to functionalize the electrode with azide groups. The ERGO provides (a) a relatively large active surface area for the attachment of PASE, which subsequently is bound with the amino-terminated capture probe, via π–π stacking, and (b) an excellent conductive interface for the redox reactions of the ECL co-reactant, as explained in our recent publication [39]. Using click

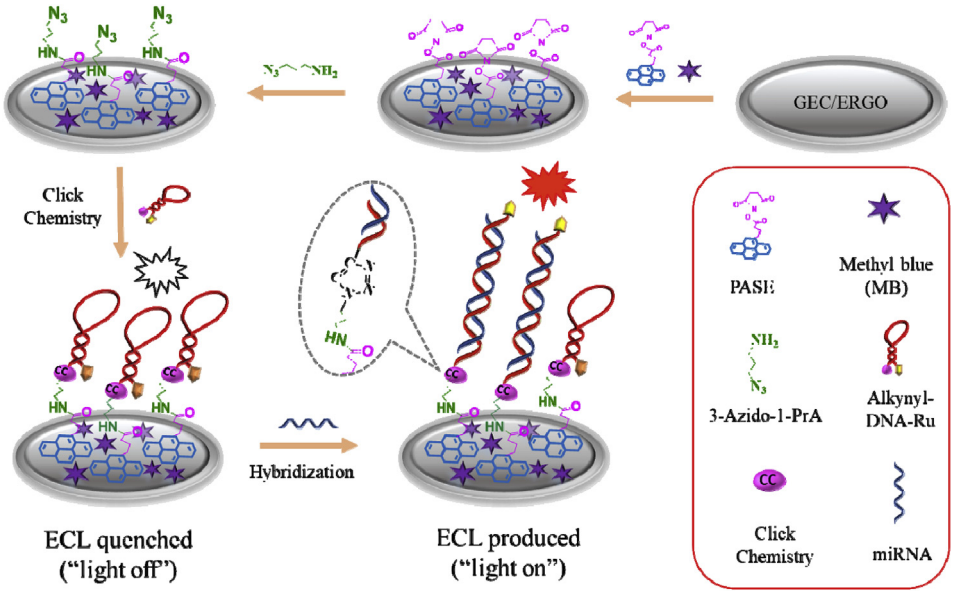

Scheme 1. Schematic diagram of constructing miRNA biosensor and its detection based on ECL quenching.

chemistry, the $Ru(bpy)_3^{2+}$ labeled alkynyl DNA hairpin probe (Alkynyl-DNA-Ru) is effectively assembled onto the electrode surface. In the presence of the anodic ECL co-reactant BDEA, the above electrode shows very weak ECL emission due to efficient ECL quenching by the surface-confined MB ("light off"). Upon the hybridization of the hairpin with the target miRNA, however, the $Ru(bpy)_3^{2+}$ emitter is separated from the MB, resulting in significant production of ECL ("light on"). Clearly, with the addition of the target analyte, the ECL signal in the present system switches from "light off" to "light on" status, which is opposite to that of the ECL quenching mode discussed previously (i.e., "light-on" to "light off").

2. Experimental section

2.1. Synthesis of the ECL hairpin probe

The ECL hairpin probe, $Ru(bpy)_2$(dcbpy)NHS-DNA (Ru-DNA) was synthesized as previously reported in the literature [40] with some modifications. Briefly, 200 μL of 1.0 mM $Ru(bpy)_2$(dcbpy)NHS in DMF was added to 50 μL of a 50 μM solution of the probe DNA. The mixture was incubated overnight with gentle shaking at RT. 100 μL NaAc (3.0 M) and 1.5 mL cold ethanol were then added successively, and the resultant solution was kept at −20 °C for 24 h to allow precipitation to occur. The solution was then centrifuged at 12,000 rpm for 30 min, and the upper yellow solution was decanted. The remaining precipitate was washed three times with 1.5 mL cold ethanol to rinse off any unbound $Ru(bpy)_2$(dcbpy)NHS. Finally, the obtained Ru-DNA precipitate was re-dissolved in 50 μL of a 5.0 mM phosphate buffer solution (PBS, pH 7.4) and stored at −20 °C prior to use.

To form the hairpin configuration, the Ru-DNA solution was warmed to and maintained at 95 °C for 5 min, and then allowed to cool to room temperature naturally over a period of 1 h.

2.2. Fabrication of the biosensor

Solutions of PASE (5.0 mM) and MB (5.0 mM) in DMF were combined in a concentration ratio of 1:3 and mixed vigorously; 10 μL of the resulting mixture was cast onto the GCE/ERGO electrode. After air-drying for 1 h, the electrode was carefully washed with 5.0 mM PBS (pH 7.4) and dried with N_2. The obtained electrode was designated as GCE/ERGO/(PASE + MB). 10 μL of 2 mM 3-azido-1-propanamine (or 3-Azido-1-PrA) was cast on the electrode to form the azido functionalized GCE/ERGO/(PASE + MB)/3-Azido-1-PrA electrode. After being air-dried for 2 h and thoroughly rinsed with 5.0 mM PBS (pH 7.4), the electrode was treated with 10 μL of the click chemistry solution [41,42], which consisted of CuSO4 (1.0 μM), TBTA (1.1 μM), and sodium L-ascorbate (2.0 μM) predissolved in a H_2O/MeOH/THF (volume mixing ratio, 2:2:1) and Ru-DNA (20 μM in 5.0 mM PBS, pH 7.4), and kept at room temperature overnight. Through this incubation process, Ru-DNA was assembled onto the azido-functionalized electrode surface via a click chemistry reaction. Unbound Ru-DNA species and other residual reagents were thoroughly removed by washing with 5.0 mM PBS (pH 7.4) to yield the fabricated miRNA biosensor, which is referred to as GCE/ERGO/(PASE + MB)/3-Azido-1-PrA/Ru-DNA in later discussion.

2.3. ECL measurements

Prior to the ECL detection, the assembled GCE/ERGO/(PASE + MB)/3-Azido-1-PrA/Ru-DNA biosensor was incubated with different concentrations of the target miRNA or a sample solution (100 μL, prepared using 0.1% (v/v) diethyl pyrocarbonate (DEPC)-treated water to inactivate possible RNase enzymes) and kept at room temperature for 30 min. After being thoroughly washed using 5.0 mM PBS (pH 7.4), the above electrode was transferred into an electrochemical cell containing 5 mL of 10 mM BDEA-0.10 M PBS (pH 7.4), and the ECL signals were measured using ECL detection via cyclic voltammetry; the electrode potential was scanned between 0.40 and 1.40 V vs Ag/AgCl at a scan rate of 0.1 V/s. For all ECL measurements, the bias voltage of the photomultiplier tube was set to 800 V.

3. Results and discussion

3.1. ECL quenching of the $Ru(bpy)_3^{2+}$/BDEA system by MB

First, the solution-phase quenching of the ECL of the $Ru(bpy)_3^{2+}$/BDEA system by MB was studied to determine the ECL quenching behavior of the surface-confined miRNA biosensor. As shown in Fig. 1A, upon the addition of MB to the $Ru(bpy)_3^{2+}$/BDEA solution, the initial ECL response of the anodic co-reactant (curve a) decreased with increasing MB concentration (curves b-d and Inset

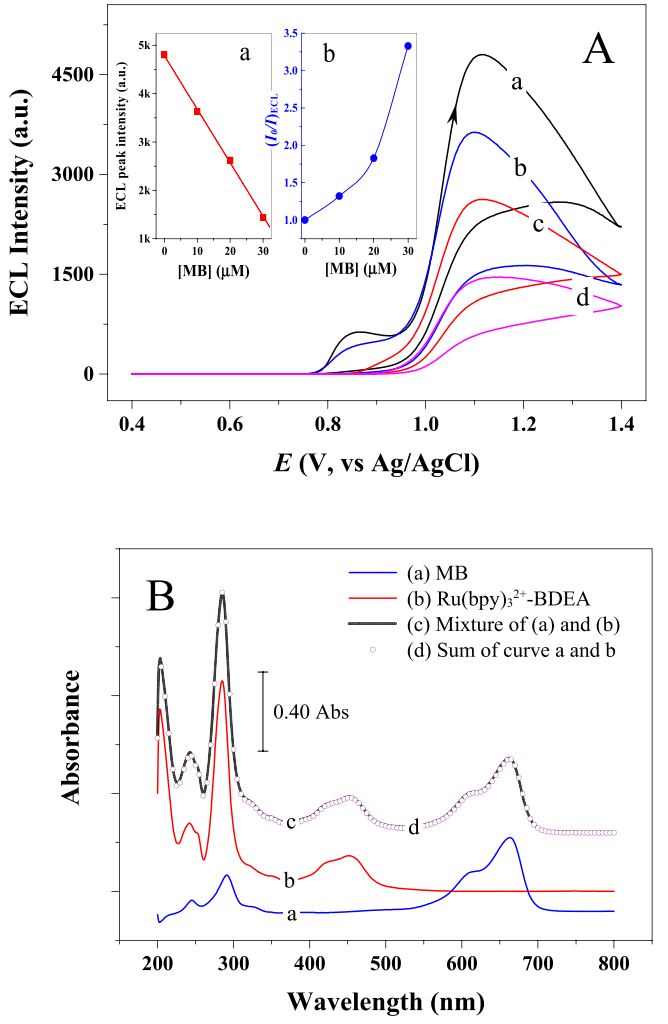

Fig. 1. (A) Effect of MB concentration on ECL intensity of the $Ru(bpy)_3^{2+}$/BDEA system at a bare GCE with a scan rate of 100 mV/s (a) 10 μM $Ru(bpy)_3^{2+}$-10 mM BDEA-0.10 M PBS (pH 7.4), (b) a +10 μM MB, (c) a +20 μM MB, and (d) a +30 μM MB. Inset: (a) Relationship of the ECL peak intensity with the MB concentration, and (b) Stern-Volmer plot of ECL quenching in which I_0 and I were the ECL peak intensity in the absence and presence of MB quencher, respectively. (B) UV–vis absorption spectra of (a) 10 μM MB, (b) 10 μM $Ru(bpy)_3^{2+}$ + 10 mM BDEA, (c) mixture of (a) and (b), and (d) sum of curve a and b. A quartz cuvette with 1.0 cm light pathlength was used.

a). The Stern-Volmer plot shown in Inset b displays an upward curvature, suggesting that the ECL quenching does not follow a simple dynamic (collisional) or static quenching process [43]. Fig. 1B shows the UV–Vis absorption spectra of (a) 10 μM MB, (b) 10 μM $Ru(bpy)_3^{2+}$-10 mM BDEA, (c) the mixture of (a) + (b), and (d) the sum of curve (a) and curve (b). The complete overlap of curve c with curve d indicates that no chemical reaction occurred when MB was mixed with the $Ru(bpy)_3^{2+}$/BDEA system. Therefore, mixing of the chemical reagents did not affect the ECL quenching. Photoluminescence quenching experiments involving $Ru(bpy)_3^{2+}$ and four anthraquinone and seven azo organic dyes revealed that no static quenching could be observed [44]. Considering the similarity of the chemical structure of MB with those of some anthraquinone dyes, such as alizarin and alizarin red S, the formation of a stable complex between excited state $Ru(bpy)_3^{2+*}$ and MB, which would be prerequisite for static quenching, is unlikely. As a result, the ECL quenching presented in this section must involve a combination of fluorescence (FL) dynamic quenching and quenching processes directly associated with the redox reactions during the ECL generation. Because the ECL-potential profile of the $Ru(bpy)_3^{2+}$/BDEA system, which includes a pre-ECL wave at around 0.85 V vs Ag/AgCl (Fig. 1A), is nearly identical to that of the classic anodic co-reactant $Ru(bpy)_3^{2+}$/TPrA (TPrA = tri-n-propylamine) system [45], the same ECL mechanism should be applicable in both cases [14,46]. Due to the insignificant contribution of the pre-wave ECL to the overall ECL quenching, the following discussion will focus on the quenching behavior related to the main ECL wave at ~1.1 V vs Ag/AgCl. The ECL is generated via the following pathways:

$$\mathrm{BDEA} \xrightarrow[-e]{0.85\ \mathrm{V}} \mathrm{BDEA}^{\bullet+} \xrightarrow{-H^+} \mathrm{BDEA}^{\bullet} \quad (1)$$

$$Ru(bpy)_3^{2+} \xrightarrow[-e]{1.15\ \mathrm{V}} Ru(bpy)_3^{3+} \quad (2)$$

$$Ru(bpy)_3^{2+} + \mathrm{BDEA}^{\bullet} \rightarrow Ru(bpy)_3^{+} + \mathrm{product} \quad (3)$$

$$Ru(bpy)_3^{3+} + \mathrm{BDEA}^{\bullet} \rightarrow Ru(bpy)_3^{2+}{}^{*} + \mathrm{product} \quad (4)$$

$$Ru(bpy)_3^{3+} + Ru(bpy)_3^{+} \rightarrow Ru(bpy)_3^{2+}{}^{*} \quad (5)$$

$$Ru(bpy)_3^{2+}{}^{*} \rightarrow Ru(bpy)_3^{2+} + h\nu\ (\sim 620\ \mathrm{nm}) \quad (6)$$

where the reversible potential for the $Ru(bpy)_3^{2+}/Ru(bpy)^{3+}$ redox couple is about −1.5 V vs Ag/AgCl [34], and the irreversible reduction potential for the BDEA• free radical is estimated to be similar to that of the TPrA• free radical, i.e., −1.7 V vs Ag/AgCl [47].

Upon the addition of MB to the $Ru(bpy)_3^{2+}$/BDEA system, the electrogenerated $Ru(bpy)_3^{2+*}$ excited state species collided with the MB molecules, resulting in partial ECL quenching (Eq. (7)). This is consistent with the fact that the FL spectrum of $Ru(bpy)_3^{2+}$ is effectively overlapped with the absorption spectrum of MB (Fig. 2). Note that the ECL spectrum of $Ru(bpy)_3^{2+}$ is well known to be essentially the same as its FL spectrum [20].

$$Ru(bpy)_3^{2+}{}^{*} \xleftarrow{\text{collision}} \mathrm{MB} \rightarrow Ru(bpy)_3^{2+} \quad (7)$$

On the other hand, MB is known to be reversibly reduced to leucomethylene blue (LCMB) through a two-electron transfer process (Eq. 8) with a pH dependent redox potential [48]; this potential is ~ -0.30 V vs Ag/AgCl in neutral media [49–53].

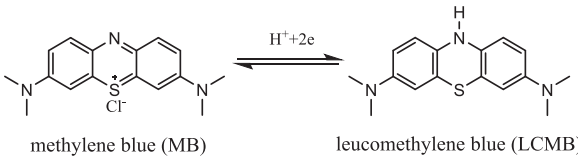

(8)

As a result, the strongly reducing species BDEA• and $Ru(bpy)_{3}+$, which are produced via Eq. (1) and Eq. (3), respectively, are consumed by the added MB through the following chemical reactions:

$$\mathrm{BDEA}^{\bullet} + \mathrm{MB} \rightarrow \mathrm{LCMB} + \mathrm{product} \quad (9)$$

$$Ru(bpy)_3^{+} + \mathrm{MB} \rightarrow Ru(bpy)_3^{2+} + \mathrm{LCMB} \quad (10)$$

Furthermore, the newly formed LCMB can be re-oxidized to MB by electrogenerated $Ru(bpy)_3^{3+}$ (Eq. (2)):

$$\mathrm{LCMB} + Ru(bpy)_3^{3+} \rightarrow \mathrm{MB} + Ru(bpy)_3^{2+} \quad (11)$$

The MB produced in this reaction can be recycled back to Eqs. (9) and (10), leading to an electrocatalytic-type reaction that causes remarkable depletion of the species that are critical to ECL generation (i.e., BDEA•, $Ru(bpy)_3^{+}$, and $Ru(bpy)_3^{3+}$) at the electrode surface. Consequently, ECL is efficiently quenched via the above-mentioned electron-transfer processes. Interestingly, instead of an upward-curving plot like that observed in the present system (Inset b of Fig. 1A), a linear Stern-Volmer plot was reported for the $Ru(bpy)_3^{2+}$/TPrA-TNT system [34]. This suggests that the reversibility of the reduction of the quencher by the free radical of the co-reactant (i.e., BDEA• or TPrA•) and $Ru(bpy)_3^{+}$ could play a key role in promoting ECL quenching associated with electron-transfer processes, given that TNT can only be irreversibly reduced. In other words, the reversible reduction is favorable for ECL quenching.

For the surface-bound Ru-DNA/BDEA-MB system, the ECL quenching should also include resonance energy transfer (RET) between the excited state ECL emitter and the surface-confined MB when the $Ru(bpy)_2(dcbpy)$ moiety is in close proximity to the electrode surface.

3.2. Electrochemical characterization and optimization of the biosensor

Fig. S2A shows the cyclic voltammograms obtained from (a)

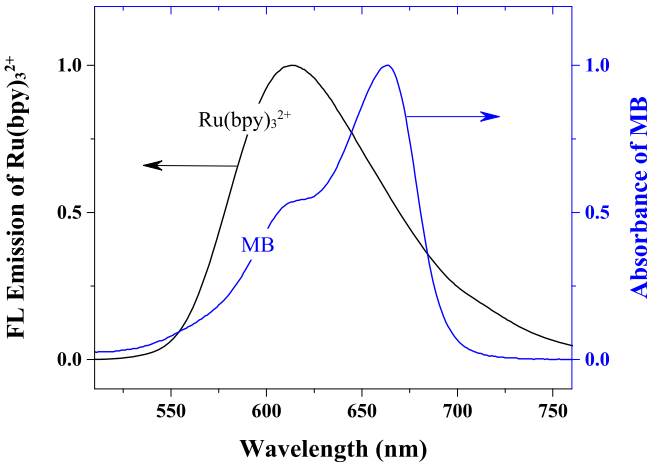

Fig. 2. Spectra overlap between the photoluminescence spectrum of $Ru(bpy)_3^{2+}$ and the absorption spectrum of MB.

bare GCE, (b) GCE/ERGO, (c) GCE/ERGO/(PASE + MB)/3-Azido-1-PrA/Ru-DNA, and (d) GCE/ERGO/(PASE + MB)/3-Azido-1-PrA/Ru-DNA/miRNA in an electrolyte solution of 5.0 mM $K_3[Fe(CN)_6]$ - 5.0 mM $K_4[Fe(CN)_6]$ in 0.10 M KCl. A slight increase in the peak current is seen after the reduced graphene oxide was electrodeposited on the GCE (curve a vs curve b), indicating the increased conductivity due to ERGO [54]. A significant decline in peak current accompanied by a small increase in the separation of the peak potentials is observed (curve c) when Ru-DNA was immobilized onto the azido-functionalized surface of GCE/ERGO/(PASE + MB)/3-Azido-1-PrA via the click chemistry reaction. This was attributed to the repulsive interaction between the negatively charged phosphate backbone of Ru-DNA and the $[Fe(CN)6]^{3-/4-}$ redox couple in the electrolyte, as well as the probable increase in the surface electric resistance or decrease in the heterogeneous electron-transfer rate. After hybridization with miRNA, the obtained GCE/ERGO/(PASE + MB)/3-Azido-1-PrA/Ru-DNA/miRNA electrode displayed a further decrease in its CV response (curve d) and a slightly larger peak potential separation as compared to those of the electrode in curve c. This was due to the formation of the double-stranded DNA-miRNA duplex, and resulted in a further increase in the negative charge density on the electrode surface.

The above stepwise functionalization of the electrode could also be monitored using electrochemical-impedance spectroscopy (EIS), as we demonstrated in a recent publication [39]. Consistent with the changes in the CV responses, the EIS results demonstrated differences in the electron-transfer resistance after each surface modification.

Several key experimental conditions the fabrication of the miRNA biosensor were examined and optimized. Fig. S2B depicts the effect of the mixing concentration or mole ratio of PASE to MB on the change in the ECL intensity (ΔECL) after the sensor was incubated with miRNA. ΔECL obviously increases with the PASE to MB mole ratio up to 1:3 and then declines. As briefly described earlier, PASE was used as a base for the azido-functionalization needed for the attachment of the Ru-DNA via click chemistry, and MB was used as an ECL quencher. Not surprisingly, the relative amounts of PASE and MB competitively adsorbed on the GCE/ERGO electrode affected the ECL detection, as raising the amount of MB could lower the background ECL signal to some extent and provide relatively abundant space for the ECL hairpin probe assemblies, which should be favorable for subsequent target miRNA hybridization and the enhancement of ECL signals. Nevertheless, further increasing the amount of MB leads to a decrease in ΔECL, probably because the reduced amount of PASE on the electrode limited the number of Ru-DNA moieties that could be attached, thus reducing the ECL signal recovery. Therefore, the optimal mixed concentration/mole ratio of PASE to MB was found to be 1:3.

The azidation degree of the electrode surface was directly determined by the amide reaction between 3-Azido-1-PrA and PASE, which further affected the click chemistry reaction and the assembly of DNA probe. Thus, two additional experimental conditions, i.e., the binding time and the concentration of 3-Azido-1-PrA on the GCE/ERGO/(PASE + MB) electrode, were also optimized. As shown in Fig. S2C(a), as the 3-Azido-1-PrA binding time increases, the ECL intensity gradually increases until 120 min, after which it levels off. Hence, 120 min was chosen for the subsequent 3-Azido-1-PrA binding processes. The effect of the 3-Azido-1-PrA concentration on ECL is shown in Fig. S2C(b), in which 2 mM is shown to be an effective concentration for miRNA biosensor fabrication.

Fig. S2D depicts the effect of the composition of the click chemistry reaction medium on the ECL response of the biosensor; the optimal mole ratio of $CuSO_4$ to sodium L-ascorbate was found to be 1:2.

3.3. Analytical detection of miRNA by the sensor

Using the optimized experimental conditions, the sensitivity of the designed sensor was tested. Fig. 3A depicts the ECL response of the biosensor to different concentrations of let-7d; the ECL intensity rises with increasing miRNA concentration from 10 fM to 10 nM. A linear relationship between the ECL peak intensity (y) and log[let-7d (pM)] (referred to as x) is shown in Fig. 3B; the linear regression equation was determined to be $y = 4322 + 896.5x$ with a correlation coefficient (R2) of 0.997. In comparison to other detection methods for miRNA (Table 1), the present sensor possesses sensitive analytical performance for detecting let-7d with a relatively low limit of detection of 10 fM (signal to noise is 3) and an attractive dynamic range of six orders of magnitude from 0.010 to 1×10^4 pM.

3.4. Specificity, reproducibility, and stability

Due to the short sequence and sequence homology of miRNA, selectivity is a vital factor when fabricating a miRNA biosensor. To assess the specificity of the present sensor, three other miRNAs from the same sequence family as let-7d, namely let-7a, let-7b, and let-7c (Table S1), were employed for the selectivity investigation. In

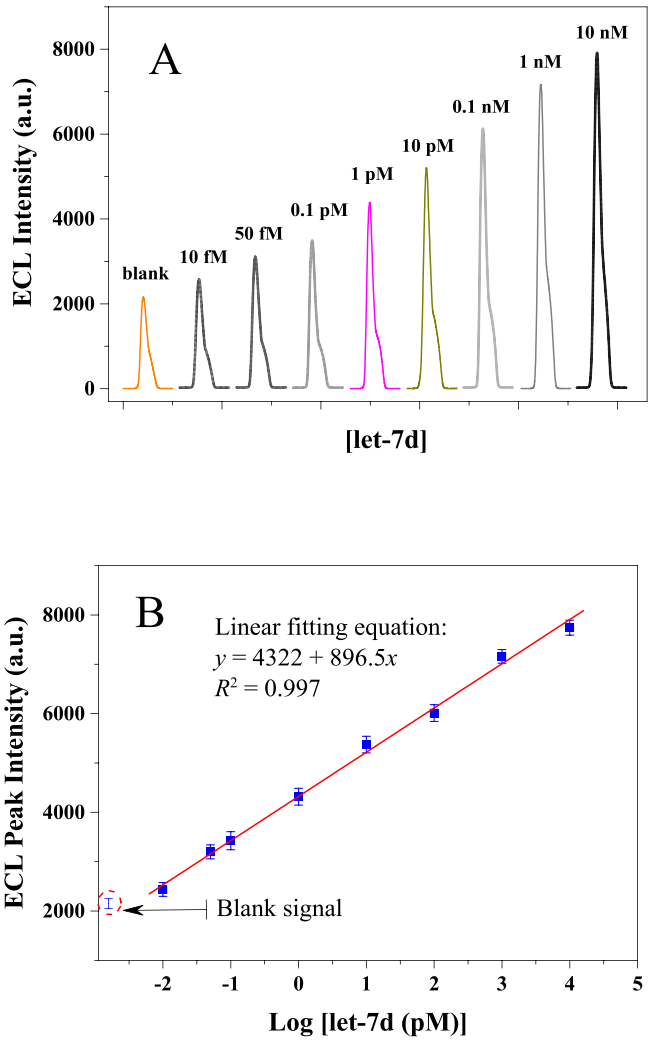

Fig. 3. (A) ECL responses of the proposed miRNA biosensor to different concentrations of let-7d, and (B) Calibration curve of the miRNA biosensor.

Table 1
Comparison between the proposed biosensor and referenced methods for detection of miRNAs.

Biosensor configuration	Detection method[a]	Linear range (pM)	Detection limit (fM)	Refs
GCE/AuNPs/DNA tweezer/report DNA	ECL	0.1×10^{-3}-10	0.03	[55]
DNA super-sandwich assemblies/streptavidin	SPR	10–1×10^{6}	9000	[56]
miRNA-21/DNA-AuNPs@MoS_2	DPV	0.01–1000	0.78	[57]
CdTe QDs/probe/Target miRNA-122	RLS	160–4800	9400	[58]
Capture probe/miRNA/detection probe	Fluorescence	0.01–100	1.38	[59]
GCE/ERGO/(PASE + MB)/3-Azido-1-PrA/Ru-DNA	ECL	0.01–10,000	10	This work

[a] SPR: surface plasmon resonance; DPV: differential pulse voltammetry; RLS: resonance light scattering.

comparison to let-7d, these three miRNAs have 2, 4, and 3 mismatched bases, respectively. Fig. 4A shows a comparison of their ECL responses; the ECL signal associated with let-7d is significantly larger than those of other three miRNA samples. Additionally, the changes in the ECL signals correlated well with the number of mismatched bases in the miRNA. When fewer mismatched bases are present, the Ru-DNA probe is more likely to hybridize with the target miRNA, leading to a greater amount of the $Ru(bpy)_2(dcbpy)$ moiety moving away from the MB quencher on electrode surface, leading to a stronger ECL response.

The reproducibility of the designed biosensor was evaluated by recording ECL signals from (a) three identical miRNA biosensing electrodes incubated with 0.10 nM of the miRNA let-7d (Fig. 4B(a)) and (b) three different measurements obtained using the same biosensor/miRNA (Fig. 4B(b)) under the same experimental conditions. Relative standard deviations (RSDs) of 3.86% and 4.05% were achieved in these experiments, respectively, indicating that the miRNA sensor possessed good reproducibility.

The long-term stability of the biosensor was studied by taking ECL measurements before and after the miRNA (i.e., let-7d) incubated electrode was stored at 4 °C for three weeks. An ECL recovery signal of 91.2% was obtained, demonstrating the excellent stability of the biosensor.

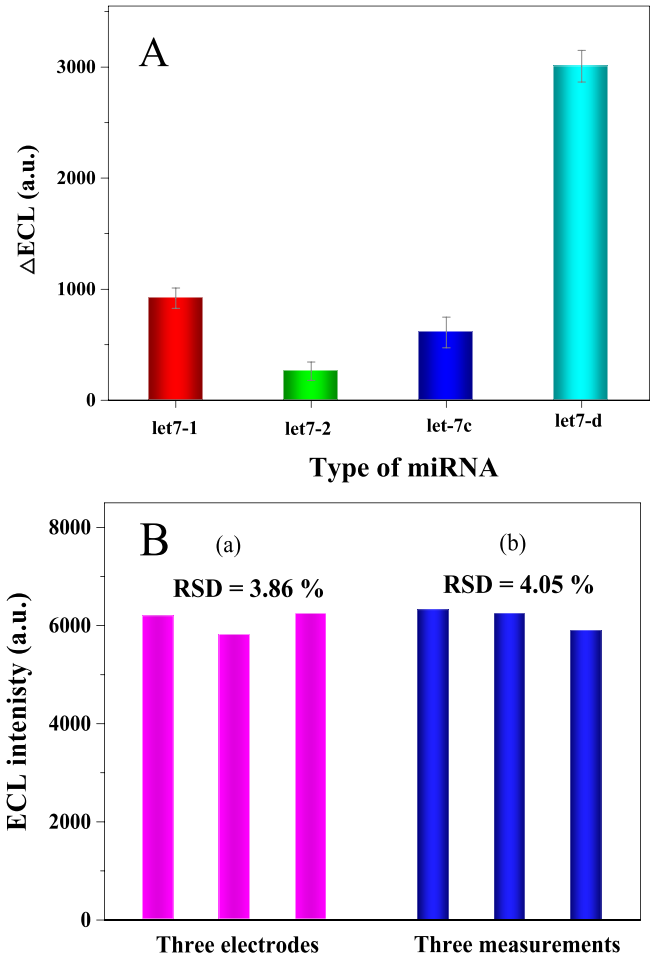

Fig. 4. (A) Integrated ΔECL intensity of the proposed biosensor after being incubated with different types of miRNAs samples at a concentration of 0.10 nM for each RNA. (B) ECL intensity of the miRNA biosensor incubated with 0.10 nM let-7d from (a) three identical electrodes, and (b) three measurements of one individual electrode. ECL was performed in 0.10 M PBS (pH 7.4) containing 10 mM BDEA at a CV scan rate of 100 mV/s.

3.5. Detection of a cell sample using the biosensor

To verify the reliability of our biosensor in the analysis of practical samples, the proposed biosensor was used to detect the concentration of let-7d extracted from A549 cells. This cell line has been widely used in studies of the miRNA let-7d [60–62]. As shown in Fig. 5, the average ECL intensities for the detection of 5×10^6, 1×10^7, and 5×10^7 cells were 3443, 3677, and 4522 (a.u.), respectively. The corresponding total let-7d concentrations were calculated to be 0.11 (±0.03), 0.19 (±0.03), and 1.67 (±0.04) pM (95% confidence interval) using the linear regression equation given in the Analytical performance of the biosensor section (Fig. 3). The data obtained using the constructed ECL biosensor indicate that it can correlate the number of cells to the target miRNA concentration (inset of Fig. 5) in the detection of real biological samples.

3.6. Estimation of the binding constant of miRNA with the immobilized Ru-DNA

One of the major assumptions for DNA probe-based biosensors

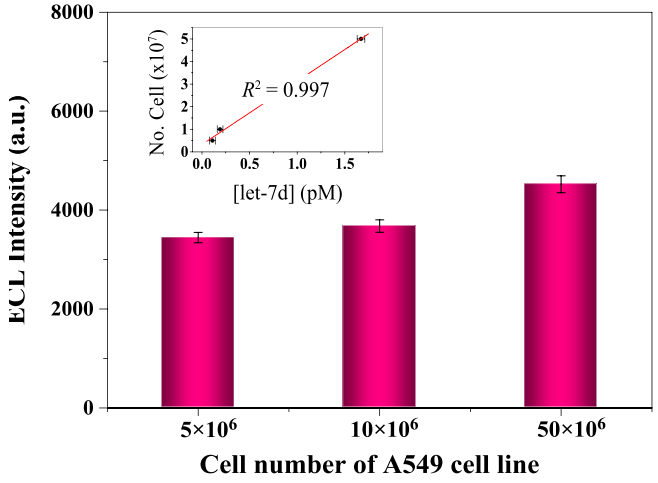

Fig. 5. Real sample analysis of let-7d detection in A549 cell lysates, performed in 0.10 M PBS (pH 7.4) containing 10 mM BDEA. Inset: relationship between the number of cells and the concentration of miRNA let-7d.

is that the probe reacts with the target to form a stable complex. However, little is known on how strong the probe-target interaction would be, especially considering the fact that the reaction process often occurs on the surface of an electrode consisting of a series of layers. In this section, we use an extended Langmuir model [63] to estimate the binding constant of the probe DNA with miRNA let-7d. Fig. S3A shows the relationship between the ECL intensity change (ΔECL) and the concentration of miRNA over a wide concentration range. Initially, the ΔECL increases sharply, but then approaches a relatively stable value in the high concentration range. Assuming the DNA-RNA hybridization process meets the requirements of the Langmuir isotherm model [19,64], the binding constant (i.e., the equilibrium constant Kb) can be expressed as:

$$\mathrm{Ru-DNA|_{GCE}} + \mathrm{miRNA} \rightleftharpoons \mathrm{Ru-DNA \bullet miRNA|_{GCE}} \quad (12)$$

$$K_b = \frac{[\mathrm{Ru-DNA \bullet miRNA|_{GCE}}]}{[\mathrm{Ru-DNA|_{GCE}}][\mathrm{miRNA}]} \quad (13)$$

Where [Ru-DNA•miRNA|GCE], [Ru-DNA|GCE], and [miRNA] represent the surface concentration of the hybridized DNA-miRNA complex on the GCE, the concentration of the capture probe Ru-DNA assembled on the GCE, and the solution concentration of the target miRNA, respectively. Thus, the relationship between ΔECL, the maximum ΔECL (ΔECLmax) corresponding to the maximum solution concentration of miRNA at saturated hybridization, the concentration of target miRNA [miRNA], and the binding constant (Kb) can be expressed as follows:

$$\Delta\mathrm{ECL} = \Delta\mathrm{ECL_{max}} \times \frac{K_b[\mathrm{miRNA}]^n}{1 + K_b[\mathrm{miRNA}]^n} \quad (14)$$

This expression can be rearranged to give Eq. (15):

$$\frac{[\mathrm{miRNA}]^n}{\Delta\mathrm{ECL}} = \frac{1}{K_b \cdot \Delta\mathrm{ECL_{max}}} + \frac{[\mathrm{miRNA}]^n}{\Delta\mathrm{ECL_{max}}} \quad (15)$$

Where the parameter n is a number related to the spread of the surface energy distribution [63]. For the Langmuir isotherm (the ideal model), n approaches unity (1) and the surface approaches homogeneity. The non-linear fit of the experimentally obtained data illustrates that the Langmuir model (i.e., Eq. (14) with n = 1) cannot be applied in the present case (Figure S3A(a)). Instead, an extended Langmuir model (Eq. (14), with three variables including n) fits the data excellently (Figure S3A(b)) to give values of ΔECLmax = 5985 (a.u.), Kb = 0.47 pM^{-1}, and n = 0.33. According to Eq. (15), [miRNA]n/ΔECL should be linearly proportional to [miRNA]n, with an intercept of 1/(Kb•ΔECL_{max}) and a slope of 1/ΔECLmax. Fig. S3B shows such a plot, where n = 0.33 from previous non-linear fitting was used. As expected, the calculated ΔECL_{max} and Kb values matched well with those obtained from Fig. S3A. The large Kb value (0.47 pM^{-1} or $4.7 \times 10^{11}\ M^{-1}$) suggests that under the present experimental conditions, the surface-confined probe DNA could bind the 22-mer miRNA let-7d strongly. This strong binding is probably responsible for the LOD and the very wide dynamic range of the present biosensor. Previous studies have shown that the binding affinities of aptamers are highly target-dependent, with binding constants ranging from 1×10^{12} to $1 \times 10^{7}\ M^{-1}$ for various targets [65–67]. The small n value is consistent with the surface property of the biosensor, in which multiple binding sites (i.e., 22 bases per DNA probe) are available for miRNA interactions. In a sense, the surface is very heterogeneous.

4. Conclusions

An ultrasensitive ECL biosensor for miRNA detection was designed based on the click ligation of a $Ru(bpy)_2(dcbpy)$-labeled DNA hairpin (Ru-DNA) and on the use of surface-confined MB molecules as ECL quenchers in the $Ru(bpy)_2(dcbpy)$/BDEA ECL system. On the basis of ECL, FL, and UV–Vis spectroscopic studies, the ECL quenching behavior of the surface-bound $Ru(bpy)_2(dcbpy)$/BDEA-MB system was attributed to a combination of the resonance energy transfer (RET), collisional (dynamic) quenching, and electron-transfer related quenching pathways. Upon hybridization of the target miRNA with the Ru-DNA hairpin, which was assembled effectively on the electrode via click chemistry, the Ru-terminal moved away from the MB-bound surface, resulting in an increase in the ECL intensity that was very sensitively correlated to the target concentration. The proposed miRNA biosensor was capable of quantifying miRNA let-7d over a very wide dynamic range from 10 fM to 10 nM. Furthermore, the biosensor demonstrated excellent specificity, remarkable reproducibility, and outstanding stability toward the target miRNA. The ECL sensing strategy presented in this paper could have great potential in the detection and quantification of biological samples. Finally, using an extended Langmuir isotherm, a strong binding constant between the DNA probe and the target miRNA let-7d was estimated.

Declaration of competing interest

The authors declare that they have no known competing financial interests or personal relationships that could have appeared to influence the work reported in this paper.

Acknowledgements

This investigation was financially supported by the National Natural Science Foundation of China (No. 21527808, 21475006), Beijing Academic Outstanding Young Scientists Projects, Beijing municipal high level innovative team building program (IDHT 20180504) and the NSF CAREER Award (CHE 0955878, WJM).

Appendix A. Supplementary data

Supplementary data to this article can be found online at https://doi.org/10.1016/j.aca.2019.09.073.

References

[1] H. Dong, J. Lei, L. Ding, Y. Wen, H. Ju, X. Zhang, MicroRNA: function, detection, and bioanalysis, Chem. Rev. 8 (2013) 6207–6233.
[2] S.M. Hammond, microRNA detection comes of age, Nat. Methods 1 (2006) 12–13.
[3] J.E. Dostie, Z. Mourelatos, M. Yang, A. Sharma, G. Dreyfuss, Numerous microRNPs in neuronal cells containing novel microRNAs, RNA 2 (2003) 180–186.
[4] Y. Wang, D.N. Keys, J.K. Au-Young, C. Chen, MicroRNAs in embryonic stem cells, J. Cell. Physiol. 2 (2009) 251–255.
[5] B. Tian, J. Ma, Z. Qiu, T. Zardán Gómez De La Torre, M. Donolato, M.F. Hansen, P. Svedlindh, M. Strömberg, F. Medicinska, O.F.V. Medicinska, G.O.P. Institutionen För Immunologi, O.F.M. Nanoteknologi, V. Teknisk-naturvetenskapliga, I. Klinisk, U. Uppsala, F.T. Institutionen, T.F. Fasta, S. Tekniska, Optomagnetic detection of MicroRNA based on duplex-specific nuclease-assisted target recycling and multilayer core-satellite magnetic superstructures, ACS Nano 2 (2017) 1798–1806.
[6] C. Ye, M.Q. Wang, H.Q. Luo, N.B. Li, Label-free photoelectrochemical "Off–On" platform coupled with G-wire-enhanced strategy for highly sensitive MicroRNA sensing in cancer cells, Anal. Chem. 21 (2017) 11697–11702.
[7] S. Monticelli, K.M. Ansel, C. Xiao, N.D. Socci, A.M. Krichevsky, T. Thai, N. Rajewsky, D.S. Marks, C. Sander, K. Rajewsky, A. Rao, K.S. Kosik, MicroRNA profiling of the murine hematopoietic system, Genome Biol. 8 (2005) R71.
[8] S. Lu, S. Wang, J. Zhao, J. Sun, X. Yang, Fluorescence light-up biosensor for MicroRNA based on the distance-dependent photoinduced electron transfer,

Anal. Chem. 16 (2017) 8429–8436.
[9] S. MansouriMajd, Abdollah Salimi, Foad Ghasemi, An ultrasensitive detection of miRNA-155 in breast cancer via direct hybridization assay using two dimensional molybdenum disulfide field-effect transistor biosensor, Biosens. Bioelectron. (2018) 6–13.
[10] T. Kangkamano, A. Numnuam, W. Limbut, P. Kanatharana, T. Vilaivan, P. Thavarungkul, Pyrrolidinyl PNA polypyrrole_silver nanofoam electrode as a novel label-free electrochemical miRNA-21 biosensor, Biosens. Bioelectron. (2018) 217–225.
[11] Z. Xu, L. Liao, Y. Chai, H. Wang, R. Yuan, Ultrasensitive electrochemiluminescence biosensor for MicroRNA detection by 3D DNA walking machine based target conversion and distance-controllable signal quenching and enhancing, Anal. Chem. 16 (2017) 8282–8287.
[12] H. Shao, J. Lu, Q. Zhang, Y. Hu, S. Wang, Z. Guo, Ruthenium-based metal organic framework (Ru-MOF)-derived novel Faraday-cage electrochemiluminescence biosensor for ultrasensitive detection of miRNA-141, Sens. Actuators B Chem. (2018) 39–46.
[13] H. Shuai, K. Huang, Y. Chen, L. Fang, M. Jia, Au nanoparticles_hollow molybdenum disulfide microcubes based biosensor for microRNA-21 detection coupled with duplex-specific nuclease and enzyme signal amplification, Biosens. Bioelectron. (2017) 989–997.
[14] C. Liu, L. Wang, L. Lu, T. Kang, MicroRNA detection by an amplification-free biosensor based on controllable solid-state electrochemiluminescence quenched by charge transfer, Anal. Methods-Uk (2017) 6760–6768.
[15] H. Huang, W. Bai, C. Dong, R. Guo, Z. Liu, An ultrasensitive electrochemical DNA biosensor based on graphene/Au nanorod/polythionine for human papillomavirus DNA detection, Biosens. Bioelectron. (2015) 442–446.
[16] H. Peng, Y. Hu, P. Liu, Y. Deng, P. Wang, W. Chen, A. Liu, Y. Chen, X. Lin, Label-free electrochemical DNA biosensor for rapid detection of mutidrug resistance gene based on Au nanoparticles/toluidine blue–graphene oxide nanocomposites, Sens. Actuators B Chem. (2015) 269–276.
[17] J.N. Murphy, A.K.H. Cheng, H. Yu, D. Bizzotto, On the nature of DNA self-assembled monolayers on Au: measuring surface heterogeneity with electrochemical in situ fluorescence microscopy, J. Am. Chem. Soc. 11 (2009) 4042–4050.
[18] F. Ricci, R.Y. Lai, A.J. Heeger, K.W. Plaxco, J.J. Sumner, Effect of molecular crowding on the response of an electrochemical DNA sensor, Langmuir 12 (2007) 6827–6834.
[19] B. Sun, H. Qi, F. Ma, Q. Gao, C. Zhang, W. Miao, Double covalent coupling method for the fabrication of highly sensitive and reusable electrogenerated chemiluminescence sensors, Anal. Chem. 12 (2010) 5046–5052.
[20] W. Miao, Electrogenerated chemiluminescence and its biorelated applications, Chem. Rev. 7 (2008) 2506–2553.
[21] F. Chowdhury, A. Williams, P. Johnson, Validation and comparison of two multiplex technologies, Luminex® and Mesoscale Discovery, for human cytokine profiling, J. Immunol. Methods 1 (2009) 55–64.
[22] R.N. Fichorova, N. Richardson-Harman, M. Alfano, L. Belec, C. Carbonneil, S. Chen, L. Cosentino, K. Curtis, C.S. Dezzutti, B. Donoval, G.F. Doncel, M. Donaghay, J. Grivel, E. Guzman, M. Hayes, B. Herold, S. Hillier, C. Lackman-Smith, A. Landay, L. Margolis, K.H. Mayer, J. Pasicznyk, M. Pallansch-Cokonis, G. Poli, P. Reichelderfer, P. Roberts, I. Rodriguez, H. Saidi, R.R. Sassi, R. Shattock, J.J.E. Cummins, Biological and technical variables affecting immunoassay recovery of cytokines from human serum and simulated vaginal fluid: a multicenter study, Anal. Chem. 12 (2008) 4741–4751.
[23] G. Toedter, K. Hayden, C. Wagner, C. Brodmerkel, Simultaneous detection of eight analytes in human serum by two commercially available platforms for multiplex cytokine analysis, Clin. Vaccine Immunol. 1 (2008) 42–48.
[24] X. Feng, N. Gan, H. Zhang, T. Li, Y. Cao, F. Hu, Q. Jiang, Ratiometric biosensor array for multiplexed detection of microRNAs based on electrochemiluminescence coupled with cyclic voltammetry, Biosens. Bioelectron. (2016) 308–314.
[25] P. Zhang, Z. Lin, Y. Zhuo, R. Yuan, Y. Chai, Dual microRNAs-fueled DNA nanogears: a case of regenerated strategy for multiple electrochemiluminescence detection of microRNAs with single luminophore, Anal. Chem. 2 (2016) 1338–1345.
[26] N. Hao, X. Li, H. Zhang, J. Xu, H. Chen, A highly sensitive ratiometric electrochemi- luminescent biosensor for microRNA detection based on cyclic enzyme amplification and resonance energy transfer, Chem. Commun. (2014) 14828–14830.
[27] G. Jie, L. Tan, Y. Zhao, X. Wang, A novel silver nanocluster in situ synthesized as versatile probe for electrochemiluminescence and electrochemical detection of thrombin by multiple signal amplification strategy, Biosens. Bioelectron. (2017) 243–249.
[28] Y. Cheng, J. Lei, Y. Chen, H. Ju, Highly selective detection of microRNA based on distance-dependent electrochemiluminescence resonance energy transfer between CdTe nanocrystals and Au nanoclusters, Biosens. Bioelectron. (2014) 431–436.
[29] L. Lu, C. Liu, T. Kang, X. Wang, G. Guo, W. Miao, In situ enhanced electrochemiluminescence based on co-reactant self-generated for sensitive detection of microRNA, Sens. Actuators B Chem. (2018) 35–41.
[30] H. Wang, L. Peng, Y. Chai, R. Yuan, High-sensitive electrochemiluminescence C-peptide biosensor via the double quenching of dopamine to the novel Ru(II)-Organic complex with dual intramolecular self-catalysis, Anal. Chem. 20 (2017) 11076–11082.
[31] W. Cao, J.P. Ferrance, J. Demas, J.P. Landers, Quenching of the electrochemiluminescence of tris(2,2'-bipyridine)ruthenium(II) by ferrocene and its potential application to quantitative DNA detection, J. Am. Chem. Soc. 23 (2006) 7572–7578.
[32] H. Zhang, F. Zuo, X. Tan, S. Xu, R. Yuan, S. Chen, A novel electrochemiluminescent biosensor based on resonance energy transfer between poly(9,9-di- n -octylfluorenyl-2,7-diyl) and 3,4,9,10-perylenetetracar-boxylic acid for insulin detection, Biosens. Bioelectron. (2018) 65–71.
[33] J. Liu, M. Cui, H. Zhou, S. Zhang, Efficient double-quenching of electrochemiluminescence from CdS:Eu QDs by hemin-graphene-Au nanorods ternary composite for ultrasensitive immunoassay, Sci. Rep. Uk 1 (2016).
[34] S. Parajuli, X. Jing, W. Miao, Electrogenerated chemiluminescence (ECL) quenching of the Ru(bpy)32+/TPrA system by the explosive TNT, Electrochim. Acta (2015) 196–201.
[35] H. Wang, Y. He, Y. Chai, R. Yuan, A super intramolecular self-enhanced electrochemiluminescence immunosensor based on polymer chains grafted on palladium, Nanocages 17 (2014) 1316–1322.
[36] S. Parajuli, W. Miao, Sensitive determination of hexamethylene triperoxide diamine explosives, using electrogenerated chemiluminescence enhanced by silver nitrate, Anal. Chem. 13 (2009) 5267–5272.
[37] K. Imai, T. Okazaki, N. Hata, S. Taguchi, K. Sugawara, H. Kuramitz, Simultaneous multiselective spectroelectrochemical fiber-optic sensor: demonstration of the concept using methylene blue and ferrocyanide, Anal. Chem. 4 (2015) 2375–2382.
[38] L. Xiaoyun, N. Yongnian, S. Kokot, An electrochemical DNA-sensor developed with the use of Methylene Blue as a redox indicator for the detection of DNA damage induced by endocrine-disrupting compounds, Anal. Chim. Acta (2015) 29–37.
[39] L. Lu, J. Wang, W. Miao, X. Wang, G. Guo, Electrogenerated chemiluminescence biosensor with a tripod probe for the highly sensitive detection of MicroRNA, Anal. Chem. 2 (2018) 1452–1459.
[40] X. Li, L. Sun, T. Ding, Multiplexed sensing of mercury(II) and silver(I) ions: a new class of DNA electrochemiluminescent-molecular logic gates, Biosens. Bioelectron. 8 (2011) 3570–3576.
[41] H. Krishna, M.H. Caruthers, Alkynyl phosphonate DNA: a versatile “Click”able backbone for DNA-based biological applications, J. Am. Chem. Soc. 28 (2012) 11618–11631.
[42] H. Zhao, R. Liang, J. Wang, J. Qiu, One-pot synthesis of GO/AgNPs/luminol composites with electrochemiluminescence activity for sensitive detection of DNA methyltransferase activity, Biosens. Bioelectron. (2015) 458–464.
[43] C. Albrecht, Joseph R. Lakowicz: principles of fluorescence spectroscopy, Anal. Bioanal. Chem. 5 (2008) 1223–1224, 3rd Edition.
[44] M. Asha Jhonsi, A. Kathiravan, G. Paramaguru, C. Manivannan, R. Renganathan, Fluorescence quenching of tris(2,2′-bipyridine)ruthenium(II) dichloride by certain organic dyes, J. Solut. Chem. 10 (2010) 1520–1530.
[45] W. Miao, J. Choi, A.J. Bard, Electrogenerated chemiluminescence 69: the tris(2,2'-bipyridine)ruthenium(II), (Ru(bpy)32+)/Tri-n-propylamine (TPrA) system RevisitedA new route involving TPrA•+ cation radicals, J. Am. Chem. Soc. 48 (2002) 14478–14485.
[46] S. Han, W. Niu, H. Li, L. Hu, Y. Yuan, G. Xu, Effect of hydroxyl and amino groups on electrochemiluminescence activity of tertiary amines at low tris(2,2'-bipyridyl)ruthenium(II) concentrations, Talanta 1–2 (2010) 44–47.
[47] R.Y. Lai, A.J. Bard, Electrogenerated chemiluminescence. 70. The application of ECL to determine electrode potentials of tri-n-propylamine, its radical cation, and intermediate free radical in MeCN/benzene solutions†, J. Phys. Chem. A 18 (2003) 3335–3340.
[48] O.S. Ksenzhek, S.A. Petrova, M.V. Kolodyazhny, Electrochemical properties of some redox indicators, Bioelectrochem. Bioenerg. (1977) 346–357.
[49] A. Matsui, E. Tanaka, H.S. Choi, V. Kianzad, S. Gioux, S.J. Lomnes, J.V. Frangioni, Real-time, near-infrared, fluorescence-guided identification of the ureters using methylene blue, Surgery 1 (2010) 78–86.
[50] S.H.D.A. Nicolai, P.R.P. Rodrigues, S.M.L. Agostinho, J.C. Rubim, Electrochemical and spectroelectrochemical (SERS) studies of the reduction of methylene blue on a silver electrode, J. Electroanal. Chem. 1 (2002) 103–111.
[51] E.M. Boon, J.K. Barton, V. Bhagat, M. Nersissian, W. Wang, M.G. Hill, Reduction of ferricyanide by methylene blue at a DNA-modified rotating-disk electrode, Langmuir 22 (2003) 9255–9259.
[52] A. Katafias, P. Kita, G. Wrzeszcz, A. Mills, Kinetics of the methylene blue oxidation by cerium(IV) in sulphuric acid solutions, Transit. Met. Chem. 1 (2007) 31–37.
[53] C.G. Pheeney, J.K. Barton, DNA electrochemistry with tethered methylene blue, Langmuir 17 (2012) 7063–7070.
[54] J. Li, L. Lu, T. Kang, S. Cheng, Intense charge transfer surface based on graphene and thymine–Hg(II)–thymine base pairs for detection of Hg 2+, Biosens. Bioelectron. (2016) 740–745.
[55] P. Zhang, Z. Li, H. Wang, Y. Zhuo, R. Yuan, Y. Chai, DNA nanomachine-based regenerated sensing platform: a novel electrochemiluminescence resonance energy transfer strategy for ultra-high sensitive detection of microRNA from cancer cells, Nanoscale 6 (2017) 2310.
[56] X. Ding, Y. Yan, S. Li, Y. Zhang, W. Cheng, Q. Cheng, S. Ding, Surface plasmon resonance biosensor for highly sensitive detection of microRNA based on DNA super-sandwich assemblies and streptavidin signal amplification, Anal. Chim. Acta (2015) 59–65.
[57] S. Su, W. Cao, W. Liu, Z. Lu, D. Zhu, J. Chao, L. Weng, L. Wang, C. Fan, L. Wang, Dual-mode electrochemical analysis of microRNA-21 using gold nanoparticle-decorated MoS 2 nanosheet, Biosens. Bioelectron. (2017) 552–559.

[58] S. Lv, F. Chen, C. Chen, X. Chen, H. Gong, C. Cai, A novel CdTe quantum dots probe amplified resonance light scattering signals to detect microRNA-122, Talanta (2017) 659–663.
[59] L. Lu, D. Tu, Y. Liu, S. Zhou, W. Zheng, X. Chen, Ultrasensitive detection of cancer biomarker microRNA by amplification of fluorescence of lanthanide nanoprobes, Nano Res. 1 (2018) 264–273.
[60] J. Takamizawa, H. Konishi, K. Yanagisawa, S. Tomida, H. Osada, H. Endoh, T. Harano, Y. Yatabe, M. Nagino, Y. Nimura, T. Mitsudomi, T. Takahashi, Reduced expression of the let-7 microRNAs in human lung cancers in association with shortened postoperative survival, Cancer Res. 11 (2004) 3753–3756.
[61] K.V. Pandit, D. Corcoran, H. Yousef, M. Yarlagadda, A. Tzouvelekis, K.F. Gibson, K. Konishi, S.A. Yousem, M. Singh, D. Handley, T. Richards, M. Selman, S.C. Watkins, A. Pardo, A. Ben-Yehudah, D. Bouros, O. Eickelberg, P. Ray, P.V. Benos, N. Kaminski, Inhibition and role of let-7d in idiopathic pulmonary fibrosis, Am. J. Resp. Crit. Care 2 (2010) 220–229.
[62] A.E. Pasquinelli, B.J. Reinhart, F. Slack, M.Q. Martindale, M.I. Kurodak, B. Maller, D.C. Hayward, E.E. Ball, B. Degnan, Conservation of the sequence and temporal expression of let-7 heterochronic regulatory RNA, Nature 2 (2000) 86–89.
[63] A. Kapoor, J.A. Ritter, An extended Langmuir model for adsorption of gas mixtures on heterogeneous surfaces, Langmuir (1990) 660–664.
[64] I. Langmuir, The adsorption of gases on plane surfaces of glass, mica and platinum, J. Am. Chem. Soc. (1918) 1361–1403.
[65] H. Du, M. Rosbash, The U1 snRNP protein U1C recognizes the 5′ splice site in the absence of base pairing, Nature 6902 (2002) 86–90.
[66] Eun Jeong Cho, Joo-Woon Lee, A.D. Ellington, Applications of aptamers as sensors, Annu. Rev. Anal. Chem. (2009) 241–264.
[67] S.M. Nimjee, C.P. Rusconi, B.A. Sullenger, Aptamers: an emerging class of therapeutics, Annu. Rev. Med. 1 (2005) 555–583.